JOURNAL OF SPACECRAFT AND ROCKETS
Vol. 43, No. 2, March–April 2006

Aerodynamic Database Development for Mars Smart Lander Vehicle Configurations

Glenn J. Bobskill* and Paresh C. Parikh†
NASA Langley Research Center, Hampton, Virginia 23681
Ramadas K. Prabhu‡
Lockheed Martin Engineering and Sciences Company, Hampton, Virginia 23681
and
Erik D. Tyler§
Swales Aerospace, Hampton, Virginia 23681

An aerodynamic database has been generated for the Mars Smart Lander shelf-all configuration. Beginning with an effort to validate the computational tools against sets of experimental data, the static aerodynamic database was constructed by correcting experimental data to Mars atmospheric flight conditions at supersonic speeds, in addition to performing discrete hypersonic analyses in the continuum and noncontinuum atmospheric regimes. Three different computational fluid dynamics codes, two based on unstructured grid technology and one an established and validated structured grid-based code, were used. As part of this database development, the results for the Mars continuum atmosphere were validated with experimental data and comparisons made where applicable. The validation with the Unitary experimental data, the use of intermediate check analyses, and the validation with the Mach 6 CF_4 experimental data provided a higher confidence in the ability of the computational analyses to provide accurate aerodynamic data for the determination of static trim characteristics for longitudinal stability within the continuum and noncontinuum atmospheric regimes. The analyses of the noncontinuum regime showed the existence of multiple trim angles of attack that can be unstable or stable trim points. These trends assisted in the development of an entry controller for a nominal trajectory.

Nomenclature

A	=	reference area, m^2
BC	=	ballistic coefficient, m/CD*A
CA	=	axial-force coefficient
CD	=	drag coefficient
Cm	=	pitching-moment coefficient
Cm_α	=	static stability derivative
CN	=	normal-force coefficient
Kn	=	Knudsen number
L/D	=	lift-to-drag ratio
M	=	Mach number
m	=	vehicle mass, kg
V	=	velocity, m/s
α	=	angle of attack, deg
β	=	sideslip angle, deg
γ	=	ratio of specific heats

Subscript

trim	=	trim condition

Introduction

THE entry, descent, and landing (EDL) phases for a Mars mission can be categorized based on first-, second-, and third-generation-type systems.[1] These categories describe the development of landing ellipses based on large-scale (hundreds of kilometers), precision (<10 km), and pinpoint distance accuracies from the desired landing site, respectively. The entry phase is defined as the region between the atmospheric interface and the supersonic parachute deployment point, whereas the descent phase is defined from that point to surface landing. Whereas the first-generation EDL system uses a ballistic entry, the second-generation system employs significant improvements in guidance and navigation methods[2,3] enabling precision entry and uses a "smart" or local surface hazard avoidance and hazard tolerance system to provide a safer landing environment. The second-generation EDL system also requires the development of a higher-fidelity trajectory simulation. The Mars Smart Lander, scheduled for deployment in 2007, will use a second-generation EDL system.

The trajectory simulation for the Mars Smart Lander (MSL) configuration series was performed using the three-degree-of-freedom (DOF) version of the POST[4] (Program to Optimize Simulated Trajectories). The POST program integrates the equations of motion and includes a set of specific constraints necessary to define the overall planetary, mission, and vehicle parameters. These models include specific science-related information of the planet Mars such as planet definition, gravity, and atmosphere, whereas other models provide specific information related to the vehicle configuration and the vehicle characteristics of motion. Examples of these models include control system emulation, guidance algorithms, navigation system, mass properties, and aerodynamics. The aerodynamics model is a database that provides aerodynamic force and moment data of a specific vehicle configuration for both the entry and descent segments of the trajectory.

The development of an entry aerodynamic database requires specific knowledge of the geometry and orientation of the vehicle in addition to the freestream quantities along a given trajectory. In accordance with the Mars Smart Lander payload and surface location requirements, a set of preliminary configurations was developed that would have favorable trim characteristics along proposed nominal and dispersed trajectories. These vehicle configurations (Fig. 1) are the axisymmetric baseline, canted-all, shelf-all, and a derivative of the shelf-all (shelf-2) tested in the NASA Ames Ballistic range

Received 17 December 2002; revision received 1 August 2004; accepted for publication 1 February 2005.

*Senior Aerospace Engineer, Vehicle Analysis Branch, Systems Analysis and Concepts Directorate. Member AIAA.
†Senior Aerospace Engineer, Configuration Aerodynamics Branch, Research and Technology Directorate. Associate Fellow AIAA.
‡Senior Aerospace Engineer. Member AIAA.
§Aerospace Engineer.

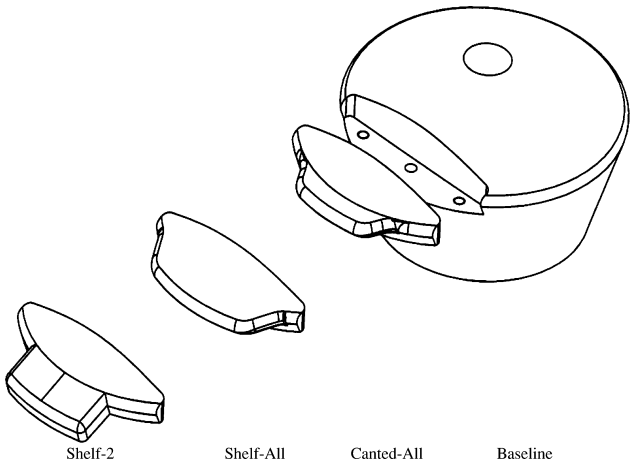

Fig. 1 Mars Smart Lander configurations.

facility. All configurations have a 70-deg forebody cone shape with a biconic backshell. The shelf-all model was designed with a blended control tab that is tangent to the forebody surface, whereas the shelf-2 model has a nonblended control tab while also being tangent to the forebody surface. The canted-all model has a tab similar to the shelf-all model, but the tab is canted 10 deg toward the vehicle nose.

The objectives of this paper are to provide an overview of the development of an entry aerodynamic database, to describe validation of the computational fluid dynamics (CFD) analysis programs with experimental data, and to show the resulting flight trim characteristics for a Mars Smart Lander configuration. The subsequent sections of this paper describe the analysis codes used, CFD validation, and the creation and results of a flight quality database.

Code Descriptions

The aerodynamic database for Mars Smart Lander was developed using three CFD codes. Two codes, USM3D and FELISA, are based on unstructured grid technology, and a third code, LAURA, is based on multiblock structured grid technology.

Unstructured Mesh Three Dimensional

Unstructured mesh three dimensional (USM3D)[5] is a three-dimensional, tetrahedral, cell-centered, finite volume Euler and Navier–Stokes flow solver for unstructured meshes. Inviscid flux quantities are computed across each cell face using Roe's flux-difference splitting.[6] Spatial discretization is accomplished using an analytical reconstruction process for computing solution gradients within tetrahedral cells. The solution is advanced in time to a steady-state condition by an implicit backward Euler time-stepping scheme. Flow turbulence is modeled by the Spalart–Allmaras one-equation model, which is optionally coupled with a wall-function formulation to reduce solution stiffness and the number of cells in the sublayer of the boundary layer. USM3D runs on massively parallel computers and clusters of personal computers. Although a single-processor version is available for a variety of computing platforms, the parallel version[7] is the code of choice because it enables rapid turnaround for large problems.

Although USM3D has been in wide use by aerospace practitioners for several years in the transonic and low supersonic regime, the latest Navier–Stokes version was never validated for the Mach-number range and shape (especially the blunt forebody) of interest in the present study. In addition, the available version has been used with perfect-gas assumptions, while the aerodynamic database required solutions at Mars atmospheric conditions involving a different gas constant. For these reasons, the flow solver had to be modified before application. The following changes were incorporated to the existing parallel version of USM3D: First, a new flow initialization procedure was introduced for the cases where the freestream Mach number exceeded 1.2; the solution was initialized to a lower, usually subsonic, value. This strategy helped the flow solution converge to steady state, especially in the aft, low-Mach-number region of the configurations. Second, a special flux-splitting scheme based on the advection upstream splitting method[8] scheme was incorporated to overcome the well-known "carbuncle phenomenon" usually associated with the application of the Roe scheme to a case with strong shock waves. And third, to simulate the Mars atmospheric conditions, the perfect-gas assumptions used thus far were modified to allow specification of an effective γ for each freestream Mach number, along with coefficients for Sutherland's law for viscosity.

LAURA

Langley aerothermodynamic upwind relaxation algorithm (LAURA)[9–11] is a three-dimensional Navier–Stokes solver for structured grids and is a finite volume formulation of the integral form of the Navier–Stokes equations. A second-order-accurate, symmetric total-variation-diminishing scheme[12] is used in conjunction with upwind differencing of the discretized equations. At each cell face, Roe's averaging defines the flowfield variables based on values from the adjacent cells. The unsteady governing equations are driven to a steady-state solution through an implicit time relaxation procedure. During the relaxation process, the grid is periodically adapted in the body-normal direction so that the grid can be tailored to the emerging solution. This elliptic flow solver has the capability of solving chemical nonequilibrium flow through the specification of chemical species and reactions unique to a specific atmosphere as well as the ability to model perfect gas and equilibrium air.

FELISA

The Finite Element Langley–Imperial College at Swansea Ames (FELISA)[13,14] software system consists of unstructured surface and volume grid generation with an inviscid flow solver and postprocessing utilities. The flow algorithm was developed through the application of the Galerkin finite element method in space to obtain a coupled set of ordinary differential equations in time. The steady-state solution of this equation set is achieved by advancing the system using an explicit Runge–Kutta-type marching scheme. The hypersonic flow solver has options for perfect gas, equilibrium air, CF_4, CO_2, and Mars equilibrium gases. In addition, the flow solver has the capability of solving chemical nonequilibrium flow and real gas (chemical and thermal nonequilibrium) flow.

Aerodynamic Database

The aerodynamic database is provided as a FORTRAN routine containing specific vehicle force and moment data as a function of vehicle orientation relative to the flow and flowfield parameters to the POST trajectory simulation. Within this routine, the vehicle trajectory is partitioned into three atmospheric regimes that are defined based on the similarity parameter of Knudsen number. The Knudsen number is defined as the mean free path (distance between molecular collisions) divided by the vehicle reference length (typically the aeroshell diameter). These atmospheric regimes are depicted in Fig. 2.

The aerodynamic database is composed of continuum, transitional, and free molecular[15,16] regimes that are accessed based on the calculated local Knudsen number at any entry trajectory point. Each section consists of axial-force, normal-force, and pitching-moment data created from specific CFD analysis points as well as experimental data[17] that have been corrected for testing environment differences. Because the trajectory simulation is normally run under nominal and off-nominal conditions during prescribed Monte Carlo analyses, the aerodynamic database has to be sufficiently populated at several freestream Mach numbers and angles of attack. To determine values within or outside the Mach number and angle-of-attack range, a biparabolic/linear interpolation/extrapolation scheme was applied.

Within the continuum regime, three different CFD analysis codes were used to obtain direct flight aerodynamic data or to provide necessary corrections to the Unitary experimental data for flight condition applicability while the noncontinuum flight data were determined using the molecular analysis code as described in Refs. 15

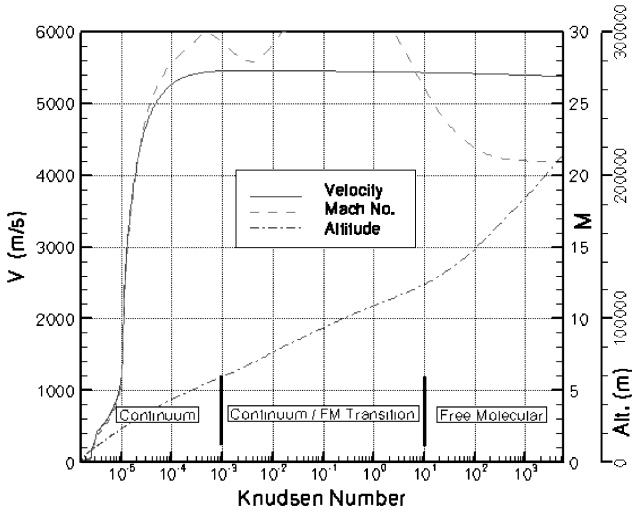

Fig. 2 Mars Smart Lander reference trajectory.

Analysis Program	M	V (m/s)
USM3D	1.6	361.37
	2.3	510.38
	3.5	755.52
	4.5	957.06
LAURA	6	1262.97
	8	1677.90
	10	2092.29
FELISA	13	2706.78
	16	3298.42
	20	4039.48
	24.5	4763.74
	28	5295.34

Fig. 3 Flight analysis cases for MSL reference trajectory.

and 16. The USM3D code was used to perform the Unitary data corrections from the predicted low supersonic parachute deploy boundary to the upper supersonic limit of the Unitary facility. The FELISA results provided the aerodynamic flight results from a mid-hypersonic to upper-hypersonic trajectory point that corresponded to the approximate atmospheric continuum limit. Last, the LAURA results provided intermediate analysis comparisons that overlap the preceding trajectory ranges. The continuum flight cases are shown in Fig. 3.

The selections and application of these analysis codes were based on several considerations. The first consideration was to develop a methodology that could allow for rapid turnaround of trend assessment for proposed vehicle configurations by taking advantage of grid-generation methods and flowfield modeling. The use of unstructured grid technology made this possible. Another consideration was the flight regime capability of each program. The final consideration was to ensure confidence and continuity within the solution matrix by using the LAURA code to validate intermediate analysis points with the USM3D and FELISA analysis programs because LAURA has been validated with previous Mars flight missions.[18]

Experimental Data

Two experimental facilities were used to acquire aerodynamic data for CFD validation and aerodatabase results. The first facility, the Langley Unitary Plan Wind Tunnel (UPWT), is a closed-circuit, continuous-flow, variable-density supersonic wind tunnel with two test sections, one with a design Mach-number range from 1.5 to 2.9 and the other with a Mach-number range from 2.3 to 4.6. The UPWT was used to obtain six-DOF static aerodynamic data for four proposed Mars Lander configurations over a Mach number range of 2.3–4.5. The complete details of the models, facility calibration, instrumentation, and data acquisition are presented in Ref. 17. The second facility, the 20-Inch Mach 6 CF4 Tunnel, used to obtain aerodynamic data for the Mars Surveyor configuration, is the only operational, conventional-type hypersonic facility in the United States that simulates dissociative real-gas phenomena associated with hypersonic flight. CF_4 test media provide a normal shock density ratio of 12 (Mach 13-18 flight), which determines real-gas effects on vehicle aerodynamics. The details of this work are presented in Ref. 19.

Results and Discussion

USM3D Validation

The USM3D code was first calibrated against the experimental data from the Unitary wind tunnel, at model scale and with the presence of the model sting. This calibrated code was subsequently used to correct (or extrapolate) the Unitary data from wind tunnel to flight. This was accomplished by obtaining the results on a configuration without the model sting and at flight Reynolds number with appropriate values for the gas constant and the Sutherland's viscosity and by correcting wind-tunnel data with increments obtained from the later simulation. Along with the changes to USM3D already described, an unstructured mesh was constructed for the baseline and shelf-all wind-tunnel and flight configurations for a series of Mach numbers between 2.3 and 4.5. The grid for the full Navier–Stokes solution varied in size typically from 1.4 million tetrahedral cells for the wind-tunnel cases to 2.6 million cells for the flight configurations. Typical surface discretization for two wind-tunnel configurations is shown in Figs. 4 and 5.

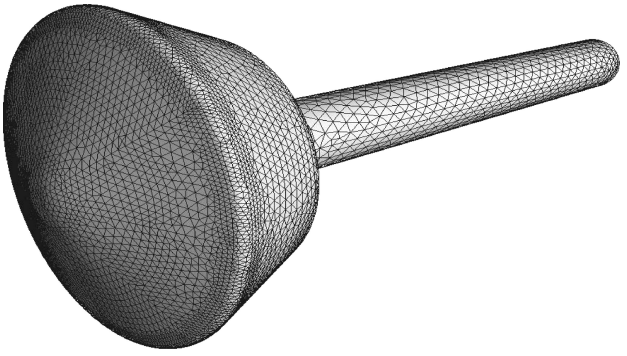

Fig. 4 Unstructured surface grid for the Unitary baseline model configuration (1.4 million cells).

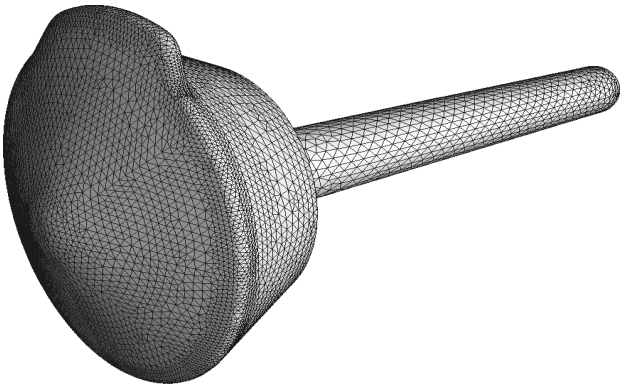

Fig. 5 Unstructured surface grid for the Unitary shelf-all model configuration.

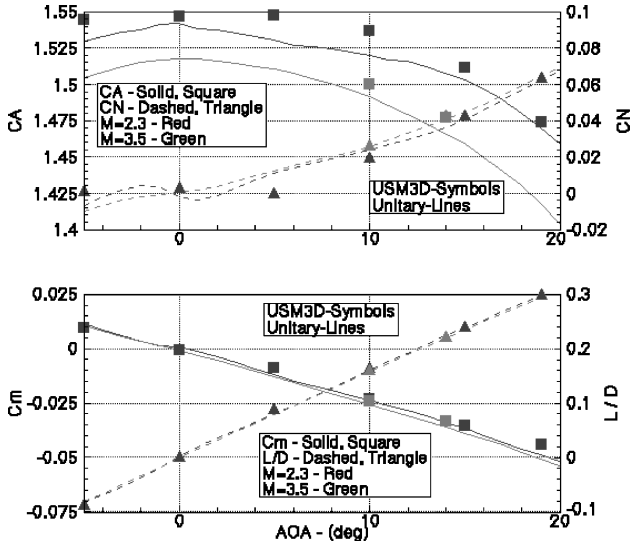

Fig. 6 USM3D/Unitary data comparisons for the baseline configuration.

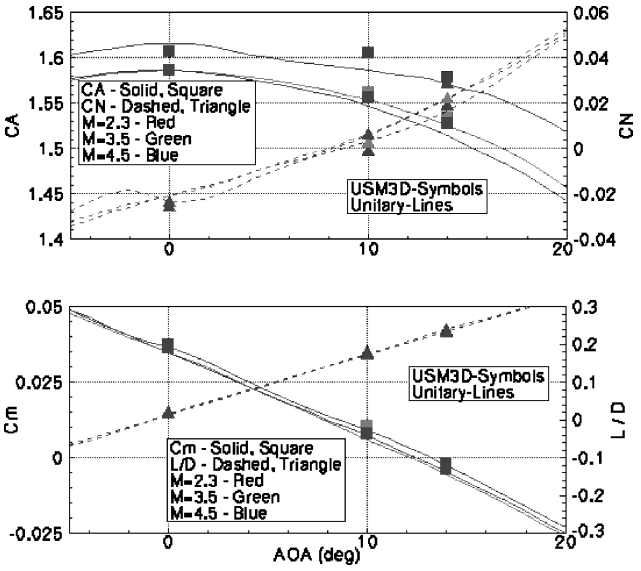

Fig. 7 USM3D/Unitary data comparisons for the shelf-all configuration.

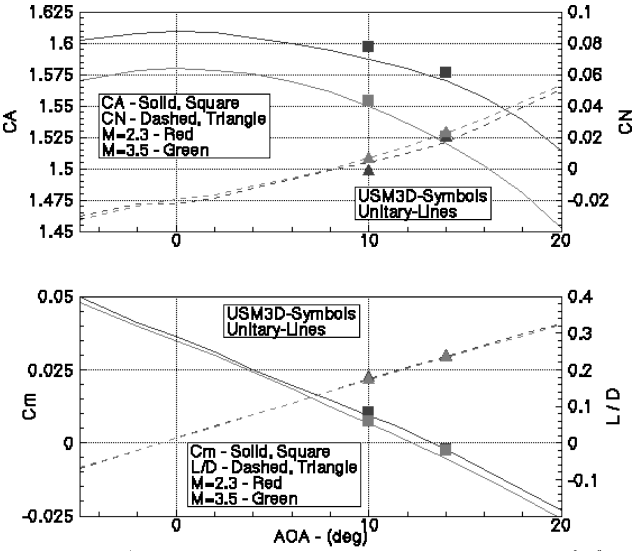

Fig. 8 USM3D/Unitary data sideslip comparisons for the shelf-all configuration ($\beta = 4$ deg).

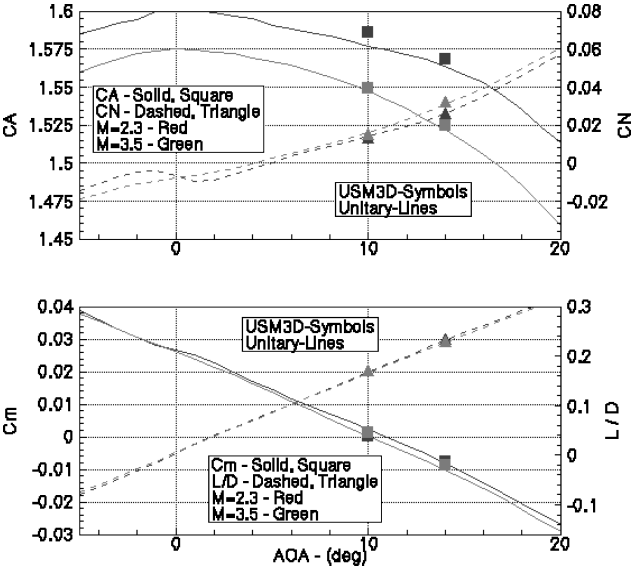

Fig. 9 USM3D/Unitary data comparisons for the canted-all configuration.

All calculations were run for a Reynolds number of 1.0×10^6 based on the maximum diameter of the configuration (0.1524 m for the wind tunnel models and 4.05 m for the flight cases) and the approximate Mars Reynolds-number value within the supersonic entry trajectory. For all computations reported here, a full viscous formulation was used.

Figure 6 for the baseline configuration shows the USM3D/Unitary comparisons for freestream Mach numbers of 2.3 and 3.5. The axial and normal forces are shown with the pitching moment (about the nose). The CFD results for the tunnel conditions ($\gamma = 1.4$) compare well against the Unitary wind-tunnel data, attesting to the accuracy of the modified solver. The detailed comparisons show a better overall agreement at the Mach 3.5 condition than at the lower Mach 2.3 condition, whereas the Mach 2.3 condition also depicts smaller differences in axial and normal force at 0 and 20 deg than the intermediate angle-of-attack range. However, the USM3D analysis does predict a change in normal force slope near zero-deg angle of attack that is a known trend for axisymmetric blunt-body configurations at low supersonic speeds.

Figure 7 shows the comparisons for the shelf-all configuration to the Unitary experimental data at freestream Mach numbers of 2.3, 3.5, and 4.5. As with the comparisons shown in Fig. 6, the overall agreement for shelf-all configuration is very good. These comparisons show better agreement in axial and normal force at lower Mach numbers than shown for the baseline model, whereas the pitching moment and L/D distribution shows excellent agreement throughout the Mach number and angle-of-attack range.

Figure 8 shows the comparisons for the shelf-all configuration to the Unitary experimental data under a sideslip condition of 4 deg. As with the preceding comparisons shown for the baseline configuration, the overall agreement for shelf-all configuration is very good. This particular case (six DOF) was chosen to increase the level of validation and thereby illustrate any deficiencies as a result of a geometry change and under sideslip conditions. These comparisons show a better agreement in axial force and a similar difference in normal force compared to the nonsideslip freestream condition. Likewise, the comparisons to the pitching moment and L/D are excellent. Further assessment of CFD validation would require some solutions at lower angles of attack, but the overall assessment is extremely good. This sideslip case was not used in the creation of the flight database that is presented in this study.

Figure 9 shows the comparisons for the USM3D canted-all configuration results to the Unitary experimental data at freestream Mach numbers of 2.3 and 3.5. As with the preceding comparisons shown

for the baseline configuration, the overall agreement for canted-all configuration is very good. These comparisons show better agreement throughout the Mach number and angle-of-attack range for all force, moment, and L/D quantities than those shown for the baseline configuration. However, additional solutions at lower angles of attack would have to be made to obtain a more complete assessment of CFD validation.

LAURA Validation

Although the LAURA analysis program has been previously validated with Mars Pathfinder hypersonic flight data,[18] an attempt was made to provide additional validation with the Unitary experimental data for a single MSL configuration at supersonic speeds and to further validate USM3D. Figure 10 shows the LAURA structured grid topology for the Unitary baseline configuration. This structured grid is composed of 16 computational blocks with an approximate total of 450,000 cell centers. In addition, this structured grid was adapted in the direction perpendicular to the body surface as a function of the flowfield temperature and using grid distribution values that maintained a corresponding boundary-layer and shock-layer grid resolution.

Figure 11 depicts the LAURA Mach-number contours for the baseline Unitary tunnel configuration for a freestream Mach number of 4.5 and an angle of attack of 10 deg with no sideslip angle. This solution imposed perfect-gas air ($\gamma = 1.4$) at $M = 4.5$ tunnel conditions with a laminar, adiabatic wall boundary conditions based on known facility operation and facility flow conditions. Figure 11 shows the general flowfield and boundary-layer characteristics of an axisymmetric blunt body with dominant subsonic regions within the shock layer, vehicle base, and sting along the vehicle symmetry and outflow planes.

Figure 12 depicts the LAURA/Unitary comparisons for the baseline Unitary tunnel configuration for freestream Mach numbers of 2.3 and 4.5. These comparisons overall show good agreement with the Unitary data for all force and pitching-moment quantities. The axial-force comparisons show better agreement at the higher angles of attack for both Mach numbers, whereas the normal-force comparison shows better agreement over the entire angle-of-attack range at Mach 4.5. The analyses performed for the 10-deg case at Mach 2.3 shows a larger difference compared to the USM3D/Unitary comparisons in Fig. 6.

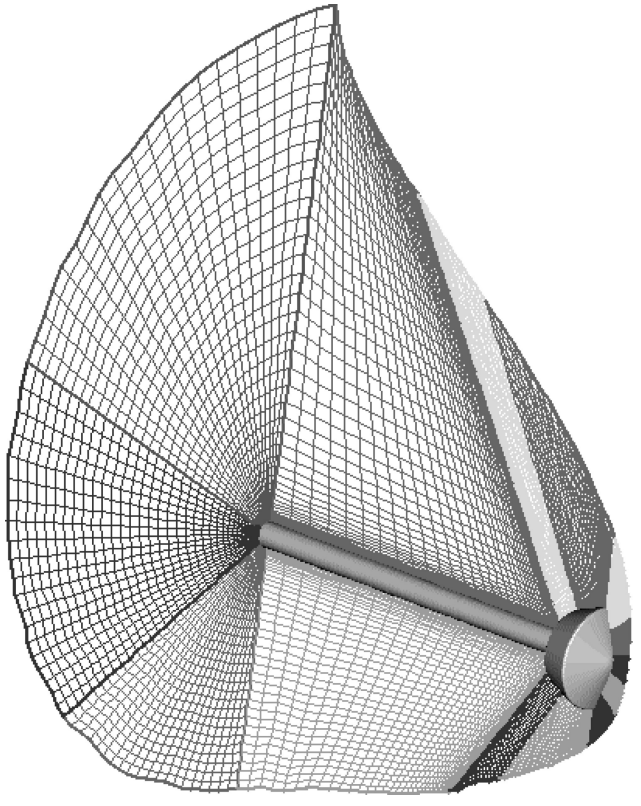

Fig. 10 Structured grid for the Unitary baseline configuration (450,000 cells).

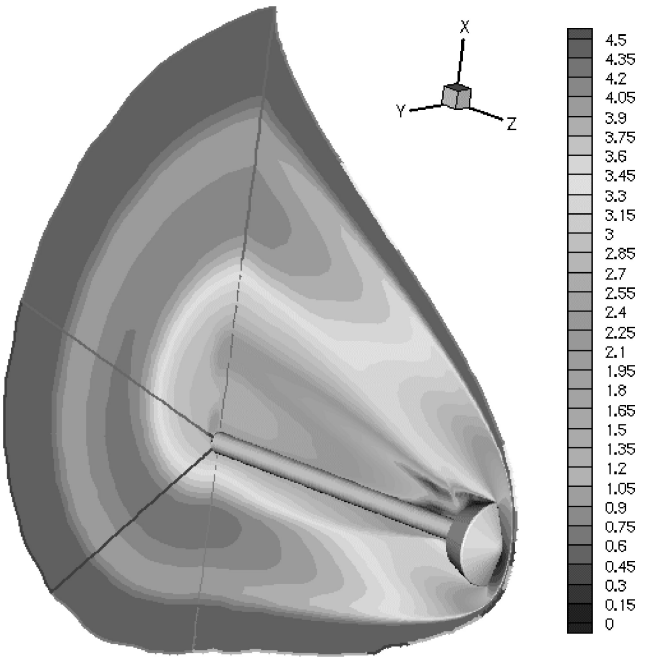

Fig. 11 Mach-number contours for the Unitary baseline configuration ($M = 4.5$; $\alpha = 10$ deg).

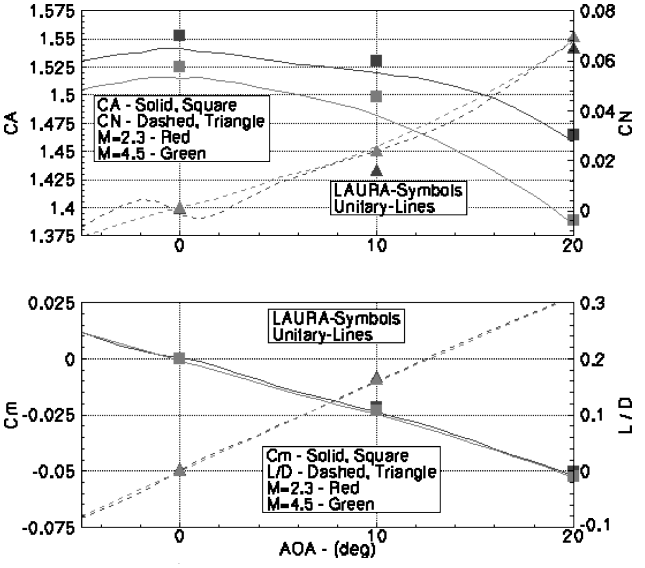

Fig. 12 LAURA/Unitary data comparisons for the baseline configuration.

FELISA Validation

The FELISA validation work was centered about an earlier Mars 2001 Surveyor configuration that was tested in the 20-inch Mach 6 CF_4 Tunnel. The Mars Surveyor configuration (Fig. 13) was similar to Mars Smart Lander configuration, but differed in the control flap geometry and location. The Mars Surveyor flap surface area was at least 50% smaller, and the flap orientation was perpendicular to the axis of rotation and located aft of the maximum diameter. The number assigned to each control flap indicated the area ratio of the flap where the larger number has a greater area ratio.

Figures 14 and 15 depict the pitching-moment coefficient and L/D ratio for the Mars Surveyor configuration for flap 1. The

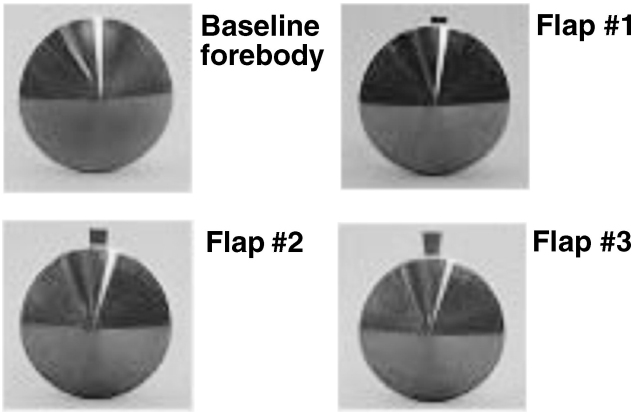

Fig. 13 Mars 2001 Surveyor wind-tunnel model.

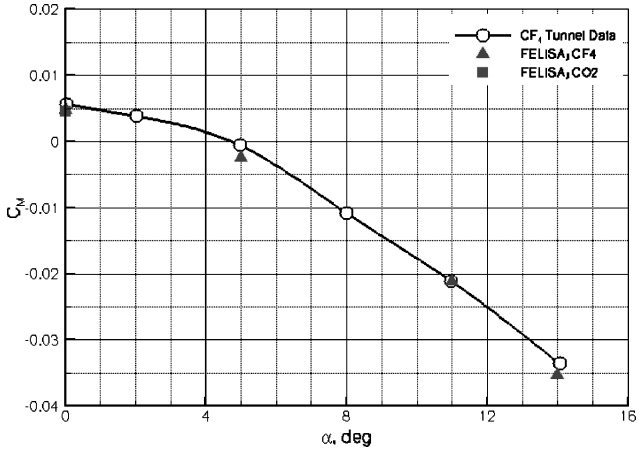

Fig. 14 FELISA/CF_4 pitching-moment comparisons for the Mars Surveyor configuration (flap 1).

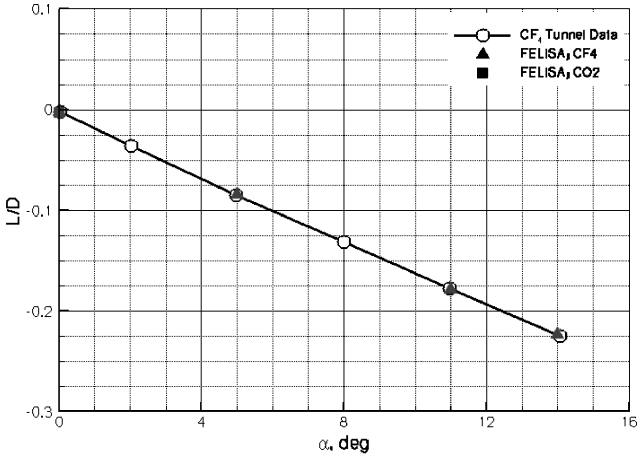

Fig. 15 FELISA/CF_4 *L/D* comparisons for the Mars Surveyor configuration (flap 1).

FELISA CF_4 results showed very good agreement to the experimental CF_4 data comparisons at 0-, 5-, 11-, and 14-deg angles of attack. In conjunction with a planned test in the 20-inch Mach 6 facility, a FELISA analysis was performed using a CO_2 test gas as a freestream condition. The FELISA results predicted that the force and moment contributions to the L/D ratio at 0-deg angle of attack would be insensitive to the CO_2 test gas. However, additional analyses at different angles of attack are necessary to determine a more generalized trend in CO_2 insensitivity.

Figures 16 and 17 depict the pitching-moment coefficient and L/D ratio for the Mars Surveyor configuration with flap 3. The

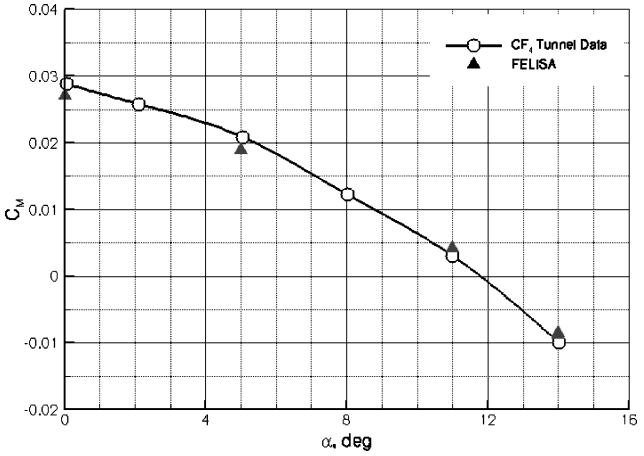

Fig. 16 FELISA/CF_4 pitching-moment comparisons for the Mars Surveyor configuration (flap 3).

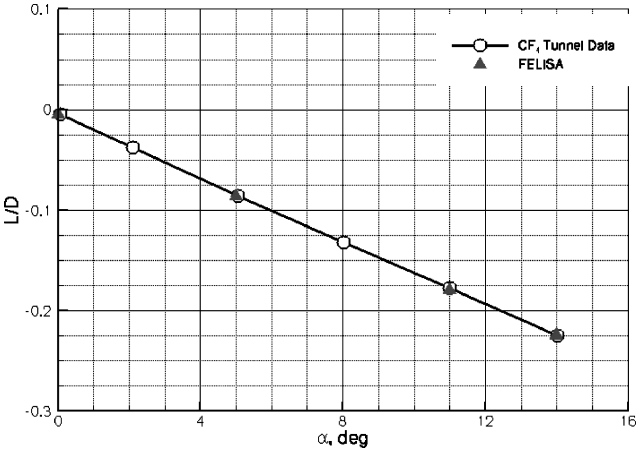

Fig. 17 FELISA/CF_4 *L/D* comparisons for the Mars Surveyor configuration (flap 3).

FELISA CF_4 results showed very good agreement with the experimental CF_4 data comparisons at 0-, 5-, 11-, and 14-deg angle of attack. The flap 3 configuration shows a slightly larger deviation in pitching moment at 0 and 5 deg as compared to the flap 1, but overall agreement is still very good. These differences could be attributed to viscous contributions (not being modeled in FELISA) induced by the larger flap or an indication of a required increase in control flap grid resolution.

Flight Results (Shelf-All Continuum Database)

For the continuum regime, an aerodynamic database was created for the Mars Smart Lander shelf-all configuration using the USM3D correction analyses for the Unitary experimental data ($M = 2.3$–4.5), the LAURA intermediate analysis check points at Mach 4.5 and 10, and the FELISA analyses at Mach 6, 8, 10, 24, and 28.

Figures 18 and 19 show the continuum trim characteristics of the shelf-all configuration based on the axial c.g. locations of (x/diameter) of 0.21 and 0.32. The c.g. of 0.21 corresponds to an early estimate of the MSL c.g. location, whereas the 0.32 value corresponds to an L/D value of approximately 0.24 at a velocity of 4700 m/s (Mach 24). In addition, the radial c.g. offset for this configuration was designed to be zero. A mass of 2200 kg was used to determine the ballistic coefficient.

At the axial c.g. of 0.21, the trim angle of attack demonstrates oscillatory behavior of 1 deg within the Mach 2.3 to 4.5 Unitary experimental data range before reaching a maximum value of 15.4 deg at a velocity of approximately 1300 m/s (Mach 6). Beyond Mach 6, the trim angle of attack at the forward c.g. exhibits a nearly linear decrease to a continuum limit value of approximately 12.8 deg. Likewise, the L/D values depict the same low supersonic behavior

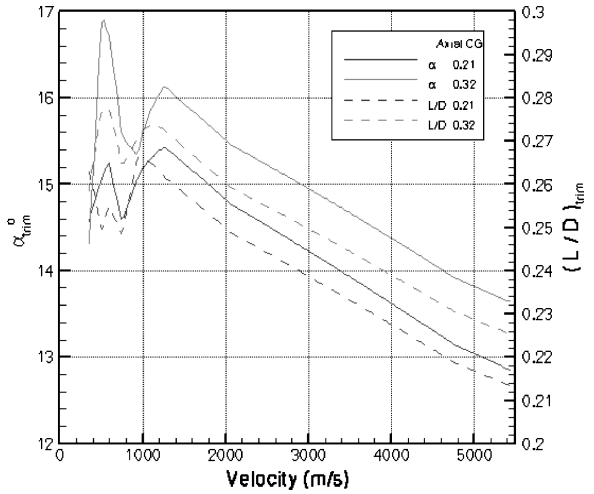

Fig. 18 *L/D* trim characteristics for shelf-all configuration.

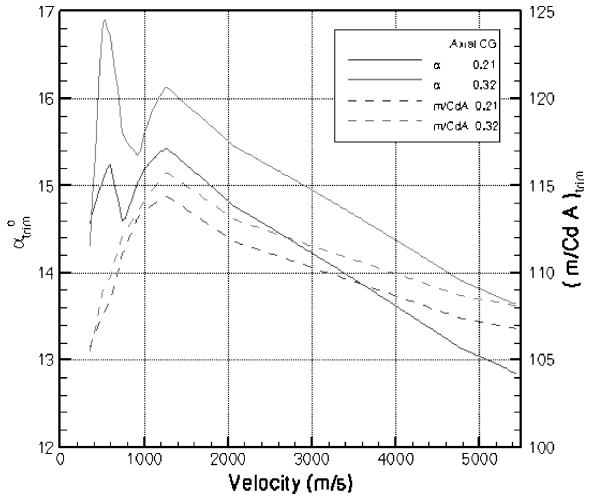

Fig. 19 Ballistic coefficient trim characteristics for shelf-all configuration (continuum).

as well as the nearly linear behavior beyond the maximum L/D of 0.266 at Mach 4.5.

At the axial c.g. of 0.32, the trim angle of attack demonstrates a larger variation in trim angle of attack of about 2.5 deg within the Unitary data range and also reached a maximum of 16.9 deg at a velocity of approximately 550 m/s (Mach 2.7) while reaching another lower peak of 16.1 deg at Mach 6. Beyond Mach 6, the trim angle of attack at the 0.32 c.g. shows a nearly linear decrease to a continuum limit value of approximately 13.6 deg. As with the forward c.g. results, the L/D shows a corresponding maximum value at the peak trim, reaching an overall maximum of 0.298.

At trim conditions, the ballistic coefficient (Fig. 19) for the forward c.g. shows no low supersonic oscillatory behavior while approaching a maximum of 114 at Mach 6 while the axial c.g. of 0.32 showed the same distribution while displaying a maximum of 116 at Mach 6. As expected, these results show a low sensitivity to CG location caused only by a small (1%) difference in ballistic coefficient over the entire continuum regime.

Flight Results (Shelf-All Noncontinuum Database)

For the rarefied regime, an existing set of free molecular data[2] over an angle-of-attack range of -180 to 180 deg was used in conjunction with a bridging function[20] to provide aerodynamic values within the transition atmospheric regime. Figures 20 and 21 show the trim characteristics for the shelf-all configuration from the edge of continuum (approximately 0.001) to a value of 20. A Knudsen number of 20 was sufficient to cover the range up to the atmospheric interface at approximately 125,000 m above ground level.

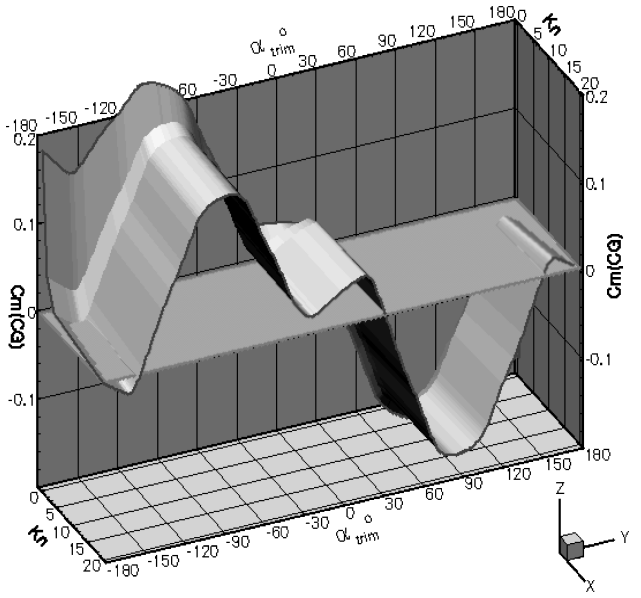

Fig. 20 Noncontinuum pitching moment for shelf-all configuration.

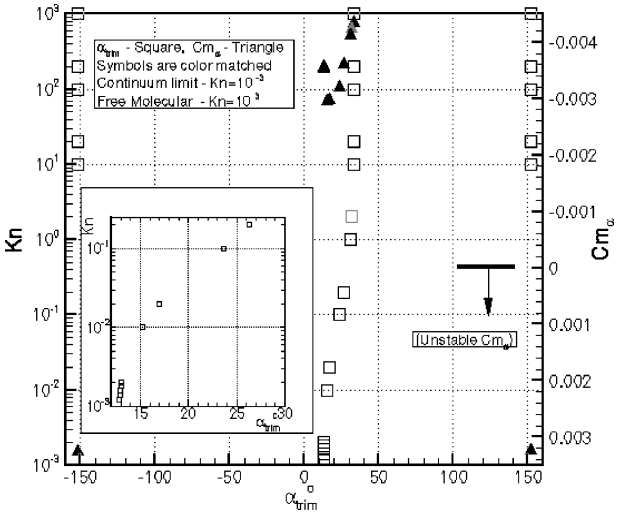

Fig. 21 Noncontinuum trim characteristics for shelf-all configuration.

Figure 20 shows the oscillatory behavior of the pitching moment within the transition regime (where the intersection of green highlighted plane represents a potential trim condition). At the continuum limit and up to a Knudsen number of approximately five, there exists a single trim point that is also stable (negative Cm_α. However, while the vehicle is traveling at the upper end of the transition regime (toward the free molecular region), for a given Knudsen number there exist multiple trim conditions, for which there can be unstable or stable trim points.

Figure 21 displays Knudsen number and Cm_α as a function of trim angle of attack α_{trim}. This figure illustrates the intersection points along the trim plane described in Fig. 20. The inserted figure shows an enlarged region of Knudsen numbers below a value of two depicting a single trim point having a stable trim condition (negative Cm_α). For Knudsen numbers above two, there exist three trim angles of which two are unstable and one is stable. These trends assisted in the development of an entry controller for a nominal trajectory for MSL. However, although the trends in the upper noncontinuum atmosphere revealed multiple trim conditions, the vehicle would be flown within a realistic flight corridor that normally would never approach these extreme angle-of-attack flight conditions.

Conclusions

The CFD validation of USM3D and LAURA with the Langley Unitary Plan Wind Tunnel experimental data, the use of intermediate

LAURA check analyses, and the validation of FELISA with the 20-Inch Mach 6 CF4 Tunnel experimental data provided very good agreement and a higher confidence in each CFD code's aerodynamic analysis results. Using these validated codes, the longitudinal static trim characteristics for the Mars continuum atmosphere were determined based on a nominal MSL trajectory. Analysis of the noncontinuum regime revealed the existence of multiple trim angles of attack that could potentially be unstable or stable trim conditions, although, as already noted, the vehicle would be flown within a realistic flight corridor.

Acknowledgments

The authors thank Steve Alter of the NASA Langley Research Center Aerothermodynamics Branch for generating the structured grids used in the LAURA analyses and providing the surface topology used for the USM3D unstructured grid generation. The authors also thank Ed Parlette of Vigyan, Inc., for creating the unstructured grids used in the USM3D analyses. In addition, thanks are due to F. McNeil Cheatwood of the NASA Langley Research Center Exploration Programs Office for his helpful recommendations and paper review.

References

[1]Lockwood, M. K., Powell, R. W., Graves, C. A., and Carman, G. L., "Entry System Design Considerations for Mars Landers," American Astronautical Society, Paper 01-023, Jan. 2001.

[2]Striepe, S. A., Queen, E. M., Powell, R. W., Braun, R. D., Cheatwood, F. M., Aguirre, J. T., Sachi, L. A., and Lyons, D. T., "An Atmospheric Guidance Algorithm Testbed for Mars Surveyor Program 2001 Orbiter and Lander," AIAA Paper 98-4569, Aug. 1998.

[3]Braun, R. D., Powell, R. W., Cheatwood, F. M., Spencer, D. A., and Mase, R. A., "The Mars Surveyor 2001 Lander: A First Step Toward Precision Landing," International Astronautical Congress, Paper IAF-98-Q.3.03, Sept. 1998.

[4]Bauer, G. L., Cornick, D. E., and Stevenson, R., "Capabilities and Applications of the Program to Optimize Simulated Trajectories (POST)," NASA CR-2770, Feb. 1977.

[5]Frink, N. T., "Tetrahedral Unstructured Navier–Stokes Method for Turbulent Flows," *AIAA Journal*, Vol. 36, No. 11, 1998, pp. 1975–1982.

[6]Roe, P. L., "Approximate Riemann Solvers, Parameter Vectors, and Difference Schemes," *Journal of Computational Physics*, Vol. 43, No. 2, 1981, pp. 357–372.

[7]Bhat, M. K., and Parikh, P. C., "Parallel Implementation of an Unstructured Grid-Based Navier–Stokes Solver," AIAA Paper 99-0663, Jan. 1999.

[8]Wada, Y., and Liou, M.-S., "An Accurate and Robust Flux Splitting Scheme for Shock and Contact Discontinuities," *SIAM Journal of Scientific Computations*, Vol. 18, No. 3, 1997, pp. 633–657.

[9]Gnoffo, P. A., "An Upwind-Biased, Point-Implicit Relaxation Algorithm for Viscous Compressible Perfect Gas Flows," NASA TP 2953, Feb. 1990.

[10]Cheatwood, F. M., and Gnoffo, P. A., "User's Manual for the Langley Aerothermodynamic Upwind Relaxation Algorithm (LAURA)," NASA TM 4674, April 1996.

[11]Riley, C. J., and Cheatwood, F. M., "Distributed-Memory Computing with the Langley Aerothermodynamic Upwind Relaxation Algorithm (LAURA)," *Advances in Engineering Software*, Vol. 29, No. 3–6, 1998, pp. 317–324.

[12]Yee, H. C., "On Symmetric and Upwind TVD Schemes," NASA TM 86842, Sept. 1985.

[13]Peiro, J., Peraire, J., and Morgan, K., "FELISA System Reference Manual and Users Guide," NASA CP-3291, May 1995.

[14]Bibb, K. L., Peraire, J., and Riley, C. J., "Hypersonic Flow Computations on Unstructured Meshes," AIAA Paper 97-0625, Jan. 1997.

[15]Wilmoth, R. G., LeBeau, G. J., and Carlson, A. B., "DSMC Grid Methodologies for Computing Low Density Hypersonic Flows About Reusable Launch Vehicles," AIAA Paper 96-1812, June 1996.

[16]Bird, G. A., *Molecular Gas Dynamics and Direct Simulation of Gas Flows*, Oxford Univ. Press, New York, 1994.

[17]Murphy, K. J., Horvath, T. J., Erickson, G. E., and Green, J. M., "Supersonic Aerodynamic Characteristics of Proposed Mars '07 Smart Lander Configurations," *Journal of Spacecraft and Rockets*, Vol. 43, No. 2, 2006, pp. 282–292; also AIAA Paper 2002-4409, Aug. 2002.

[18]Gnoffo, P. A., Braun, R. D., Weilmuenster, K. J., Mitcheltree, R. A., Engelund, W. C., and Powell, R. W., "Prediction and Validation of Mars Pathfinder Hypersonic Aerodynamic Database," *Journal of Spacecraft and Rockets*, Vol. 36, No. 3, 1999, pp. 367–373.

[19]Horvath, T. J., O'Connell, T. F., Cheatwood, F. M., Prabhu, R. K., and Alter, S. J., "Experimental Hypersonic Aerodynamic Characteristics of the Mars Surveyor 2001 Precision Lander with Deployable Flap," *Journal of Spacecraft and Rockets*, Vol. 43, No. 2, 2006, pp. 270–281; also AIAA Paper 2002-4408, Aug. 2002.

[20]Celenligil, M. C., Moss, J. N., and Blanchard, R. C., "Three-Dimensional Flow Simulation About the AFE Vehicle in the Transitional Regime," AIAA Paper 89-0245, Jan. 1989.

M. K. Lockwood
Guest Editor